Design and Stability of Voltage-Modulated Direct Power Control for Weak Grid-Connected Voltage Source Inverters

[1]Ms. Kadam Pooja Babasaheb and [2]Prof. Dr. B.M. Patil

[1]M. Tech (Control System Engineering), Department of PG, M. B. E. S. College of Engineering, Ambajogai, India

[2]Department of PG, M. B. E. S. College of Engineering, Ambajogai, India

Email Id: Poojabkadam1997@gmail.com

***Abstract*: In the weak grid –connected voltage source inverters the PLL system may make the system unstable if the conventional vector current control (VCC) method is applied, we design a voltage modulated direct power control (VM-DPC) for a three – phase voltage source inverter. In the proposed system of VM-DPC method the PLL method is eliminated as compared with the existing VCC method. When the rated real power injected to the weak grid, the VSI should generate some certain amount of reactive power too. In certain operating range, an eigen value based analysis shows the system with the proposed method tracks is desired dynamics. The simulation results match the theoretical expectations closely.**

Keywords: Voltage source inverter, voltage modulated direct Power control (VM-DPC), vector current controller, weak grid, stable system.

I. Introduction

In voltage modulated direct power control voltage source converters (VSCs) are widely used in the application of smart grid, flexible AC transmission system and renewable energy sources in the modern power grids[1]-[7]. The grid connected voltage sources inverter (VSI) is one of the key devices in VSCs, which is normally controlled as a current source injecting current into the grid. To provide satisfactory control performance for grid –connected VSIs, the conventional vector current control strategy is typically used [8]. It has been notified that a weak grid-connected VSI with the standard vector current control strategy suffers from stability and performance issue [9]-[12]. With the increasing market penetration of renewable energy resources in modern power grids, it becomes major important to sustain stability and high power quality induced by grid-connected VSIs [13].

The vector current control is a broadly used control scheme for VSIs, where the phase locked loop (PLL) is used for the purpose of grid synchronization [14]. Fig. 1 shows a Simplified vector current control structure of a single-line diagram three-phase voltage source inverter connected to a weak grid. In current years, on the small signal stability of VSIs, the bad effects of the PLL have been reported. It is stated that the PLL may regress the stability of VSIs by introducing the negative incremental resistance at low frequencies [15]-[17]. The frequency coupling dynamics of VSIs introduced by the PLL have also been clearly displayed [18]. By the bandwidth of the PLL, the frequency range of the negative resistance is determined. So, in order to improve the stability robustness of VSIs the low bandwidth PLL is usually adopted which to place in danger the dynamic performance of the system significantly. But it is still very difficult for VSIs to remain stable under the weak grid condition, goes through the PLL is designed with a very low bandwidth, in which the grid impedance is being soon to appear 1.3pu [19].

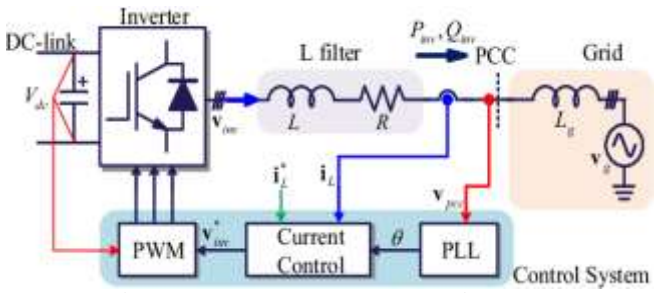

Fig. 1. Simplified vector current control structure of a single-line diagram three-phase voltage source inverter connected to a weak grid.

Freshly, in modern power grids Wang and Blaabjerg abstracted the harmonic stability caused by the grid-connected VSIs [20], where the small-signal dynamics of VSIs tend to introduce a negative damping, which may be in different frequency ranges, depending on both the specific controllers of the converters and power system conditions[19]-[23]. Therefore, the control strategy without the PLL is needed, in order to guarantee stable operations of VSIs under the weak grid conditions.

Direct power control (DPC) is another control method, it has been researched to control the instantaneous real and reactive powers directly for grid-connected VSIs without using neither inner-loop current regular nor PLL system [24], [25].However a variable switching frequency based on the switching state, is the main disadvantage of these methods, which results in an unexpected broadband harmonic spectrum i.e., it is not easy to design a line filter properly, various DPC strategies have been proposed to achieve a constant switching frequency. Few of them are using space

vector modulation [25], [26] or in each switching period calculating the required converter voltage vector [27],[28].

In addition, a sliding mode control is applied to DPC method, with the consideration of robustness, in order to guarantee a fast tracking performance of the real and reactive powers [29], and by considering the system's intrinsic dissipative nature a passivity-based control via DPC proposed [30]. Still there are undesirable repulse in both real and reactive powers. Model predictive control (MPC-DPC), one of the optimal control algorithms , by considering the multi-variable case , nonlinearities and system constraints in an intuitive way has been designed [31]-[35]. MPC-DPC selects voltage vector sequence and calculates the duty cycles, in every sampling period; it provides a constant switching frequency as well. But, it may incur additional computational burden.

Recently, Gui. et. al. solved the main disadvantage of the DPC method, he introduced a grid voltage modulated – direct power control(GVM-DPC) for the steady-state performance [36]-[37]. For the grid-connected VSIs, it may be easily designed and analyzed, through various linear control techniques since a linear time invariant(LTI) system is obtained based on GVM-DPC concept[38],[39]. However, it starts from a strong assumption that it needs a non distorted grid voltage for the GVM-DPC method. Consequently, in this proposed system, the point of common coupling (PCC) voltage is affected by the injected current from VSIs; we will show how to use GVM-DPC method in a weak grid.

In the three phase VSI connected to a weak grid, we design a voltage modulated direct power control (VM-DPC) strategy, where the PLL system may make the system unstable as discussed before. In this proposed system, the PLL is eliminated is the main advantage of this method. In order to use the concept of GVM-DPC, to apply the similar concept, we use a band-pass filter (BPF) for a weak grid connected VSI system. Additionally, in order to inject the rated real power to the weak grid, to support the voltages at the PCC as well, the system also generates some amount of reactive power. The thesis presents the system modeling of the grid-connected VSI based on the DPC model and the GVM-DPC based on BPF, a stability analysis for the whole system including the BPF with consideration of the parameter variations, simulation results using MATLAB/simulink, simscape power system and experimental test using a 15-KW-inverter system, conclusions of this work, results and references.

II. METHODOLOGY

A. Modeling of Grid-Connected Voltage Source Inverters

In this chapter, a DPC modeling of VSC is briefly introduced at first. After that, to make it to become an LTI system a VM-DPC is proposed for the VSI system.

In this study, we assume that to the dc side of the inverter a stiff dc source (V_{dc}) is connected, e.g., a dc-dc converter in a PV application or a rectifier in wind application. Hence, in this paper the dynamic from the dc input is not considered. In addition, at the grid-side a grid impedance (L_g) is considered. Fig. 1. shows a Simplified vector current control structure of a single-line diagram three-phase voltage source inverter connected to a weak grid. Normally, to synchronize the VSI with the grid through the PLL, the voltages at the PCC, (V_{pcc}) are measured. For the current control, to generate the voltage references for the PWM, either the proportional + integral (PI) controller in the dq–frame or the proportional + resonant (PR) controller in the αβ–frame could be applied. In this study, with the proposed method we only compare the PI controller in the dq–frame.

The dynamic equations consisting of the output voltages of the VSI, the voltages at the PCC, and the output currents can be expressed as follows:

$$\begin{aligned} L\frac{di_{L,a}}{dt} &= -Ri_{L,a} + v_{inv,a} - v_{pcc,a}, \\ L\frac{di_{L,b}}{dt} &= -Ri_{L,b} + v_{inv,b} - v_{pcc,b}, \\ L\frac{di_{L,c}}{dt} &= -Ri_{L,c} + v_{inv,c} - v_{pcc,c}, \end{aligned} \tag{1}$$

Where

$$\begin{aligned} v_{pcc,a} &= L_g\frac{di_{L,a}}{dt} + v_{g,a}, \\ v_{pcc,b} &= L_g\frac{di_{L,b}}{dt} + v_{g,b}, \\ v_{pcc,c} &= L_g\frac{di_{L,c}}{dt} + v_{g,c}, \end{aligned} \tag{2}$$

Where $i_{L,abc}, v_{g,abc}, v_{inv,abc}$ are the output current, the grid voltage, and the output voltage of the VSI in the abc frame, respectively. L and R are the filter inductance and resistance, respectively. Based on a balanced grid voltage condition, by using Clark transformation, the dynamic equations in (1) can be transformed into the stationary reference frame as follows:

$$\begin{aligned} L\frac{di_{L,\alpha}}{dt} &= -Ri_{L,\alpha} + v_{inv,\alpha} - v_{pcc,\alpha}, \\ L\frac{di_{L,\beta}}{dt} &= -Ri_{L,\beta} + v_{inv,\beta} - v_{pcc,\beta}, \end{aligned} \tag{3}$$

where $i_{L,\alpha\beta}, v_{pcc,\alpha\beta}$ and $v_{inv,\alpha\beta}$ indicate the output currents, the voltages at the PCC, and the inverter output voltages in the αβ–frame, respectively.

In (2), we observe that the voltages at the PCC are affected by the injected currents. However, from a non-distorted voltage the GVM-DPC proposed in [37] starts. Consequently, if
we only consider at PCC a fundamental frequency of the voltage, and then the injected currents will be the fundamental ones as well. It is acceptable since in the grid from the grid side the fundamental of real and reactive powers are expected to be injected. Hence, to obtain the
Fundamental component of the measured PCC voltages we will use a band-pass-filter (BPF).

$$v_{pcc,\alpha\beta_f} = G_{bpf} * v_{pcc,\alpha\beta}, \tag{4}$$

Where $G_{bpf}$the transfer is function of the BPF and $v_{pcc,\alpha\beta_f}$ is the fundamental component of the measured voltages at the PCC. Consequently, we can obtain the instantaneous

fundamental real and reactive powers injected from VSI to the grid in the stationary reference frame as follows [40], [41]:

$$P_f = \frac{3}{2}\left(v_{pcc,\alpha_f} i_{L,\alpha} + v_{pcc,\beta_f} i_{L,\beta}\right),$$
$$Q_f = \frac{3}{2}\left(v_{pcc,\beta_f} i_{L,\alpha} - v_{pcc,\alpha_f} i_{L,\beta}\right), \quad (5)$$

where P_f and Q_f indicate the fundamental component of the instantaneous real and reactive powers injected into the grid, respectively. Differentiating (5) with respect to time, we can obtain the dynamics of the instantaneous real and reactive powers as follows:

$$\frac{dP_f}{dt} = \frac{3}{2}\left(i_{L,\alpha}\frac{dv_{pcc,\alpha_f}}{dt} + v_{pcc,\alpha_f}\frac{di_{L,\alpha}}{dt} + i_{L,\beta}\frac{dv_{pcc,\beta_f}}{dt} + v_{pcc,\beta_f}\frac{di_{L,\beta}}{dt}\right)$$
$$\frac{dQ_f}{dt} = \frac{3}{2}\left(i_{L,\alpha}\frac{dv_{pcc,\beta_f}}{dt} + v_{pcc,\beta_f}\frac{di_{L,\alpha}}{dt} - i_{L,\beta}\frac{dv_{pcc,\alpha_f}}{dt} - v_{pcc,\alpha_f}\frac{di_{L,\beta}}{dt}\right) \quad (6)$$

Since v_{pcc} is a fundamental part of the PCC voltages, we can obtain the following relationship such as

$$v_{pcc,\alpha_f} = V_{pcc_f}cos(\omega_f t),$$
$$v_{pcc,\beta_f} = V_{pcc_f}sin(\omega_f t), \quad (7)$$

Where V_{pcc_f} is the magnitude of the fundamental PCC voltages, $V_{pcc_f} = \sqrt{v^2{}_{pcc,\alpha_f} + v^2{}_{pcc,\beta_f}}$. ω_f is the angular frequency of the fundamental PCC voltages and ω_f = 2πf, and f is the fundamental frequency of the grid voltage. Differentiating (7) with respect to time, we can obtain instantaneous fundamental PCC voltage dynamics as follows:

$$\frac{dv_{pcc,\alpha_f}}{dt} = -\omega_f V_{pcc_f} sin(\omega_f t) = -\omega_f v_{pcc,\beta_f},$$
$$\frac{dv_{pcc,\beta_f}}{dt} = \omega_f V_{pcc_f} cos(\omega_f t) = \omega_f v_{pcc,\alpha_f}, \quad (8)$$

Substituting (3) and (8) into (6), the state-space models of the fundamental real and reactive powers are generated as follows [29]:

$$\frac{dP_f}{dt} = -\frac{R}{L}P_f - \omega_f Q_f + \frac{3}{2L}\left(v_{pcc,\alpha_f} v_{inv,\alpha} + v_{pcc,\beta_f} v_{inv,\beta} - V^2_{pcc_f}\right),$$
$$\frac{dQ_f}{dt} = \omega_f P_f - \frac{R}{L}Q_f + \frac{3}{2L}\left(v_{pcc,\beta_f} v_{inv,\alpha} - v_{pcc,\alpha_f} v_{inv,\beta}\right), \quad (9)$$

Note that the dynamics of instantaneous real and reactive powers in (9) are a multi-input-multi-output (MIMO) system, where $v_{inv,\alpha}$ and $v_{inv,\beta}$ are the control inputs, P_f and Q_f are the outputs. Moreover, notice that the system is a time-varying one since both control inputs are multiplied by the grid voltages.

Fig. 2. shows block diagram the proposed method for the weak grid-connected voltage source inverter.

To simplify the dynamics in (9), we define a VM-DPC input as follows:

B. Controller Design

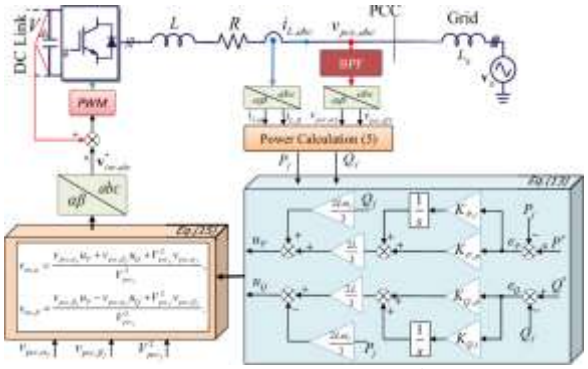

Fig. 2. Block diagram the proposed method for the weak grid-connected voltage source inverter.

$$u_P := v_{pcc,\alpha_f} v_{inv,\alpha} + v_{pcc,\beta_f} v_{inv,\beta} - V^2_{pcc_f},$$
$$u_Q := v_{pcc,\beta_f} v_{inv,\alpha} - v_{pcc,\alpha_f} v_{inv,\beta}, \quad (10)$$

where u_P and u_Q are the new control inputs, which will be designed. With the new control inputs defined in (10), the dynamics of the real and reactive powers in (9) can be rewritten as follows:

$$\frac{dP_f}{dt} = -\frac{R}{L}P_f - \omega Q_f + \frac{3}{2L}u_P,$$
$$\frac{dQ_f}{dt} = \omega P_f - \frac{R}{L}Q_f + \frac{3}{2L}u_Q, \quad (11)$$

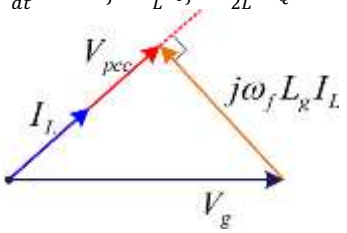

Fig. 3. phasor diagram of the voltages at PCC and grid when operating at unity power factor.

Note that the dynamics of the real and reactive powers in (11) are changed into a linear time-invariant (LTI) MIMO system with the coupling states, which has a simple structure like the model of d–q axes currents of VSI.

Let's define the errors of the real and reactive powers as follows:

$$e_P := P^* - P_f,$$
$$e_Q := Q^* - Q_f, \quad (12)$$

Where P^* and Q^* are the references of the real and reactive powers, respectively. In order to cancel the coupling terms in (11), a simple controller consisting of feed-forward and PI feedback is designed as follows:

$$u_P = \frac{2L\omega_f}{3}Q_f + K_{P,p}e_P + K_{P,i}\int_0^t e_P(\tau)d\tau,$$
$$u_Q = -\frac{2L\omega_f}{3}P_f + K_{Q,p}e_Q + K_{Q,i}\int_0^t e_Q(\tau)d\tau, \quad (13)$$

Where$K_{P,p}$, $K_{P,i}$, $K_{Q,p}$, and $K_{Q,i}$ are the PI controller gains. Substituting (13) into (11), the error dynamics of real and reactive powers could be obtained as

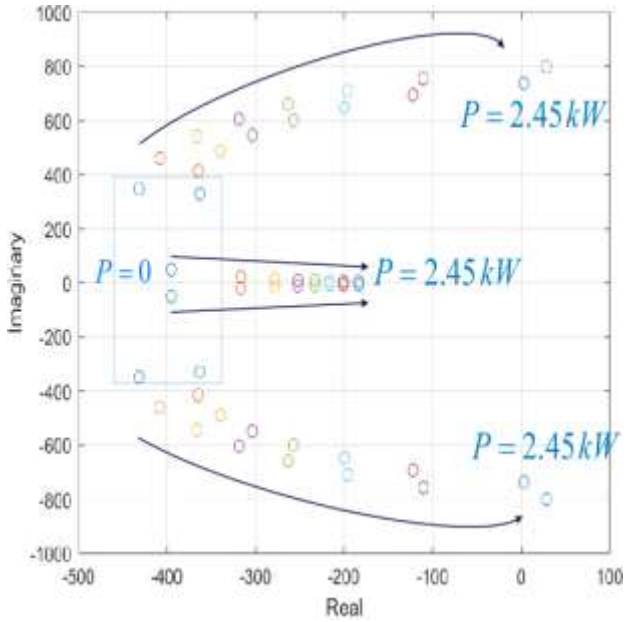

Fig. 4. Eigenvalues of the error dynamics when the real power increases from P*=0 to P*=2.45 kW and $L_g = 22mH$.

$$\dot{e}_P = -\left(K_{P,p} + \frac{R}{L}\right)e_P - K_{P,i}\int_0^t e_P(\tau)d\tau,$$
$$\dot{e}_Q = -\left(K_{Q,p} + \frac{R}{L}\right)e_Q - K_{Q,i}\int_0^t e_Q(\tau)d\tau, \quad (14)$$

Roughly, the closed-loop system with the proposed method is exponentially stable in the operating range if the PI controller gains are positive. Finally, the original control inputs, $v_{inv,\alpha}$ and $v_{inv,\beta}$, could be calculated by means of (10) as follows:

$$v_{inv,\alpha} = \frac{v_{pcc,\alpha_f}u_P + v_{pcc,\beta_f}u_Q + V_{pcc_f}^2 v_{pcc,\alpha_f}}{V_{pcc_f}^2},$$

$$v_{inv,\beta} = \frac{v_{pcc,\beta_f}u_P - v_{pcc,\alpha_f}u_Q + V_{pcc_f}^2 v_{pcc,\beta_f}}{V_{pcc_f}^2}. \quad (15)$$

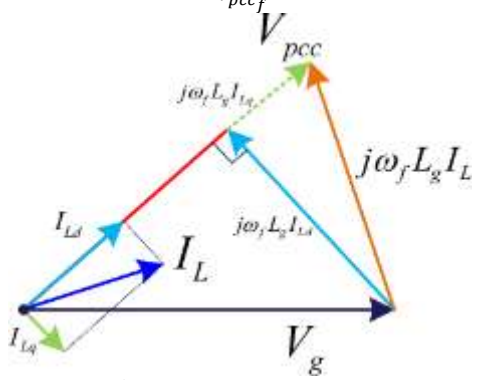

Fig. 5. Phasor diagram of the voltages at PCC and grid with consideration of reactive power [42].

III. Stability Analysis

In this section, we investigate the Eigen values of the error dynamics with the proposed method. Based on such eigen values, we analyze the stability of the weak grid-connected VSI.

At first, let us define the transfer function of the BPF used in this study as follows:

$$G_{bpf} = \frac{2\omega_c s}{s^2 + 2\omega_c s + \omega_0^2}, \quad (16)$$

Where $\omega_c = \zeta\omega_0$ is the resonance bandwidth, ω_0 is the resonance frequency, and ζ is damping ratio. To obtain the state space model of the BPF, we define the new state $x_{bpf} \in \mathbb{R}^4$, the control inputs $u_{bpf} = \left[v_{pcc,\alpha},\ v_{pcc,\beta}\right]^T$, and the output $y_{bpf} = \left[v_{pcc,\alpha_f},\ v_{pcc,\beta_f}\right]^T$, then the state-space model of the BPF can be obtained as follows:

$$\dot{x}_{bpf} = \begin{bmatrix} -2\omega_c & -\omega_0^2 & 0 & 0 \\ 1 & 0 & 0 & 0 \\ 0 & 0 & -2\omega_c & -\omega_0^2 \\ 0 & 0 & 1 & 0 \end{bmatrix} x_{bpf} + \begin{bmatrix} 1 & 0 \\ 0 & 0 \\ 0 & 1 \\ 0 & 0 \end{bmatrix} u_{bpf},$$
$$y_{bpf} = \begin{bmatrix} 2\omega_c & 0 & 0 & 0 \\ 0 & 0 & 2\omega_c & 0 \end{bmatrix} x_{bpf}. \quad (17)$$

To simplify the analysis, we use the proportional controller instead of the PI controller in (13). In order to obtain the closed-loop system, we substitute (15) and (17) into (3). Finally, we can obtain the closed-loop system as

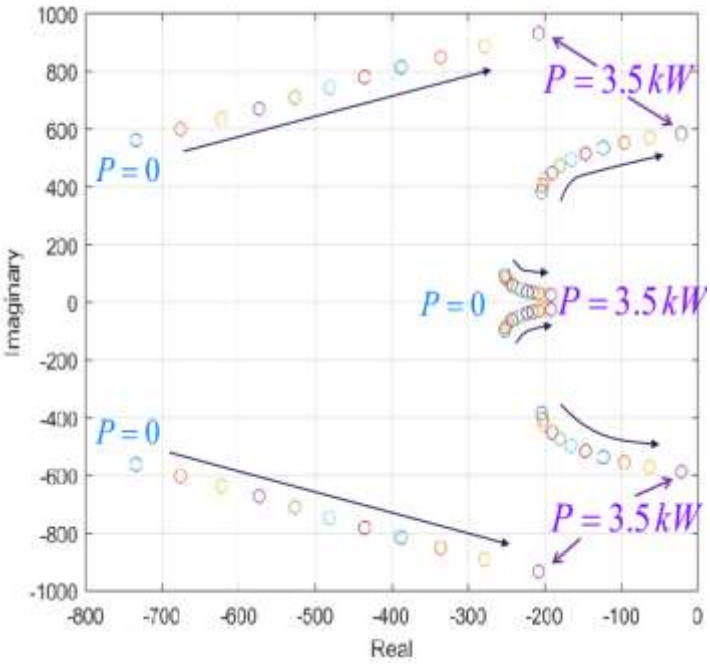

Fig. 6. Eigen values of the error dynamics when the real power increases from $P^d = 0$ to $P^d = 3.5$kW and $Q^d = 2$kvar.

$$\dot{x} = A(x)x + Bu, \quad (18)$$

Where $x = \left[i_\alpha,\ i_\beta,\ x_{bpf}\right]^T \in \mathbb{R}^6$ and $u = \left[v_{g,\alpha},\ v_{g,\beta}\right]^T \in \mathbb{R}^2$. Moreover, A and B are listed in (19) at the bottom of the paper. Since the state variables are ac signals, the error dynamics is used to consider its tracking behavior, which has only one equilibrium point at the origin.

$$A(x) = \begin{bmatrix} \frac{-R-\frac{3}{2}K_{P,p}}{L+L_g} & -\frac{L\omega_f}{L+L_g} & \frac{2\omega_c}{L+L_g}\left(1+\frac{K_{P,p}P^*}{V_{pccf}^2}\right) & 0 & \frac{2\omega_c}{L+L_g}\left(\frac{K_{P,p}Q^*}{V_{pccf}^2}\right) \\ \frac{L\omega_f}{L+L_g} & \frac{-R-\frac{3}{2}K_{Q,p}}{L+L_g} & -\frac{2\omega_c}{L+L_g}\left(\frac{K_{Q,p}Q^*}{V_{pccf}^2}\right) & 0 & \frac{2\omega_c}{L+L_g}\left(1+\frac{K_{P,p}P^*}{V_{pccf}^2}\right) \\ \frac{-R-\frac{3}{2}K_{P,p}}{L+L_g}L_g & -\frac{L\omega_f}{L+L_g}L_g & \frac{2\omega_c\left(1+\frac{K_{P,p}P^*}{V_{pccf}^2}\right)}{L+L_g}L_g - 2\omega_c & -\omega_0^2 & \frac{2\omega_c\left(\frac{K_{Q,p}Q^*}{V_{pccf}^2}\right)}{L+L_g}L_g \\ 0 & 0 & 1 & 0 & 0 \\ \frac{L\omega_f}{L+L_g}L_g & \frac{-R-\frac{3}{2}K_{Q,p}}{L+L_g}L_g & \frac{2\omega_c\left(\frac{K_{Q,p}Q^*}{V_{pccf}^2}\right)}{L+L_g}L_g & 0 & \frac{2\omega_c\left(1+\frac{K_{P,p}P^*}{V_{pccf}^2}\right)}{L+L_g}L_g - 2\omega_c \\ 0 & 0 & 0 & 0 & 1 \end{bmatrix}$$

$$B = \begin{bmatrix} -1 & 0 & 1-L_g & 0 & 0 & 0 \\ 0 & -1 & 0 & 0 & 1-L_g & 0 \end{bmatrix}^T. \quad (19)$$

We assume that there exists signal x^d to satisfy the following relationship:

$$\dot{x}^d = A(x^d)x^d + Bu, \quad (20)$$

Where $x^d = \left[i_\alpha^d,\ i_\beta^d,\ x_{bpf}^d\right]^T \in \mathbb{R}^6$. The superscript "d" indicates the desired value. The assumption in (20) is acceptable in this study, since we consider that the system dynamics are sufficiently smooth in an open connected set.

It should be noted that the proposed method stabilizes the system exponentially based on (14), i.e., P_f and Q_f converge to their references exponentially. Hence, in this study, we do not consider the dynamics of V_{pccf}^2 in (19), i.e., $V_{pccf}^2 \approx V_{pccf}^{d2}$. It is acceptable since V_{pccf}^2 is a dc value and has a slow dynamics compared to the currents. If we define an error as follows:

$$e = x^d - x, \quad (21)$$

then, the error dynamics could be obtained as,

$$\dot{e} = \dot{x^d} - \dot{x} = A(x^d)\, e \quad (22)$$

where $A(x^d)$ is listed in (23) at the bottom of the paper.

$$A(x^d) = \begin{bmatrix} \frac{-R-\frac{3}{2}K_{P,p}}{L+L_g} & -\frac{L\omega_f}{L+L_g} & \frac{2\omega_c}{L+L_g}\left(1+\frac{K_{P,p}P^d}{V_{pccf}^{d2}}\right) & 0 & \frac{2\omega_c}{L+L_g}\left(\frac{K_{P,p}Q^d}{V_{pccf}^{d2}}\right) \\ \frac{L\omega_f}{L+L_g} & \frac{-R-\frac{3}{2}K_{Q,p}}{L+L_g} & -\frac{2\omega_c}{L+L_g}\left(\frac{K_{Q,p}Q^d}{V_{pccf}^{d2}}\right) & 0 & \frac{2\omega_c}{L+L_g}\left(1+\frac{K_{P,p}P^d}{V_{pccf}^{d2}}\right) \\ \frac{-R-\frac{3}{2}K_{P,p}}{L+L_g}L_g & -\frac{L\omega_f}{L+L_g}L_g & \frac{2\omega_c\left(1+\frac{K_{P,p}P^d}{V_{pccf}^{d2}}\right)}{L+L_g}L_g - 2\omega_c & -\omega_0^2 & \frac{2\omega_c\left(\frac{K_{Q,p}Q^d}{V_{pccf}^{d2}}\right)}{L+L_g}L_g \\ 0 & 0 & 1 & 0 & 0 \\ \frac{L\omega_f}{L+L_g}L_g & \frac{-R-\frac{3}{2}K_{Q,p}}{L+L_g}L_g & \frac{2\omega_c\left(\frac{K_{Q,p}Q^d}{V_{pccf}^{d2}}\right)}{L+L_g}L_g & 0 & \frac{2\omega_c\left(1+\frac{K_{P,p}P^d}{V_{pccf}^{d2}}\right)}{L+L_g}L_g - 2\omega_c \\ 0 & 0 & 0 & 0 & 1 \end{bmatrix} \quad (23)$$

Consequently, we could consider $V_{pcc,f}$ based on a phasor diagram, as shown in Fig.3. It should be noted that upper-case letters are used for magnitude and lower-case letters are used for instantaneous variables in this study. We define V_{pcc}, V_g, and I_L, being the magnitude of v_{pcc} v_g, and i_L, respectively. From Fig. 3, V_{pcc}^d has a relationship between V_g and I_L^d such As

$$V_{pcc}^{d2} = V_g^2 - \left(\omega_f L_g I_L^d\right)^2 \quad (24)$$

If we consider the only real power, then we can obtain the following relationship such as

$$I_L^d = \frac{2}{3}\frac{P^d}{V_{pcc}}, \quad (25)$$

Substituting (25) into (24), Vpcc can be obtained as

$$V_{pcc}^{d2} = \frac{V_g^2}{2} \pm \sqrt{\frac{V_g^4}{4} - \left(\frac{2}{3}\omega_f L_g P^d\right)^2} \quad (26)$$

When $P^d = 0, V_{pcc}^d$ should be equal to V_g. Hence, it should be '+' in (26). Notice that, $\frac{V_g^4}{4} - \left(\frac{2}{3}\omega_f L_g P^d\right)^2$ should be larger than zero since V_{pcc}^{d2} should have real value. That means the inverter has a maximum real power injecting to the weak grid, which has been discussed in [42].

To analyze the weak-grid connected VSI, we assume that the capacity of the VSI is 3.5 kW. Consequently, we obtain L_g = 22 mH when SCR = 1.5 and the root mean square (RMS) of the grid voltage, $V_{ga,rms}$, is 110 V. In addition, the BPF is designed as follows: $\omega_0 = 2\pi f$ and ζ= 0.707. Fig. 4. shows the eigenvalues of the closed-loop system in (22) when the real power increases from P^d = 0 to P^d= 2:45 kW. In this case, we fix $K_{P,p} = K_{Q,p}$= 20. We can observe that the eigen values of the closed–loop system move to the right-half-plane when we increase of the real power.

To inject the rated real power to the weak grid, the reactive power should generate to compensate the voltage at the PCC [42]. Consequently, (26) is changed into relationship in (27) based on the phasor diagram, as shown in Fig. 5.

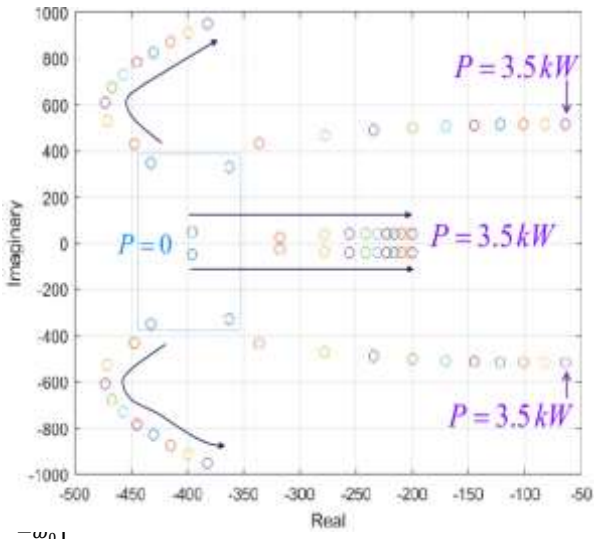

Fig. 7. Eigen values of the error dynamics when the real power increases from $P^d = 0$ to $P^d = 3.5kW$ and $Q^d = P^d$.

$$V_{pcc}^{d2} = \frac{V_g^2 + \frac{4}{3}\omega_f L_g Q^d}{2} + \sqrt{\frac{\left(V_g^2 + \frac{4}{3}\omega_f L_g Q^d\right)^2}{4} - \left(\frac{2}{3}\omega_f L_g\right)^2 (P^{d2} + Q^{d2})} \quad (27)$$

From (27), it should be noted that the following constraint should be satisfied.

$$\frac{\left(V_g^2 + \frac{4}{3}\omega_f L_g Q^d\right)^2}{4} - \left(\frac{2}{3}\omega_f L_g\right)^2 (P^{d2} + Q^{d2}) \geq 0, \quad (28)$$

Thus, the amount of reactive power to be injected for stable operation could be calculated as

$$Q^d \geq \frac{\left(\frac{2}{3}\omega_f L_g P^d\right)^2 - V_g^4}{\left(\frac{2}{3}\omega_f L_g V_g^2\right)^2} \quad (29)$$

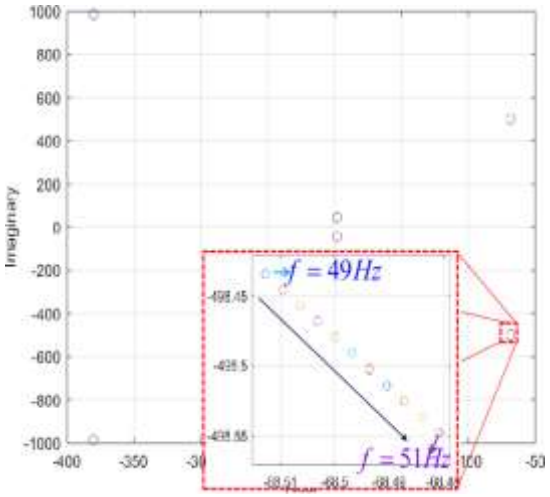

Fig. 8. Eigen values of the error dynamics when the grid frequency is changed from 49Hz to 51Hz, and $P^d = 3.5kW$ and $Q^d = P^d$.

Fig. 6. shows the eigen values of the closed-loop system in (22) when the real power increases from P^d = 0 to P^d = 3.5 kW, and Q^d = 2 kvar. In this case, the inverter could inject its rated power with the compensation of the reactive power. The eigen values of the closed-loop system move close to imaginary axis when the more real power is injected into the weak grid.

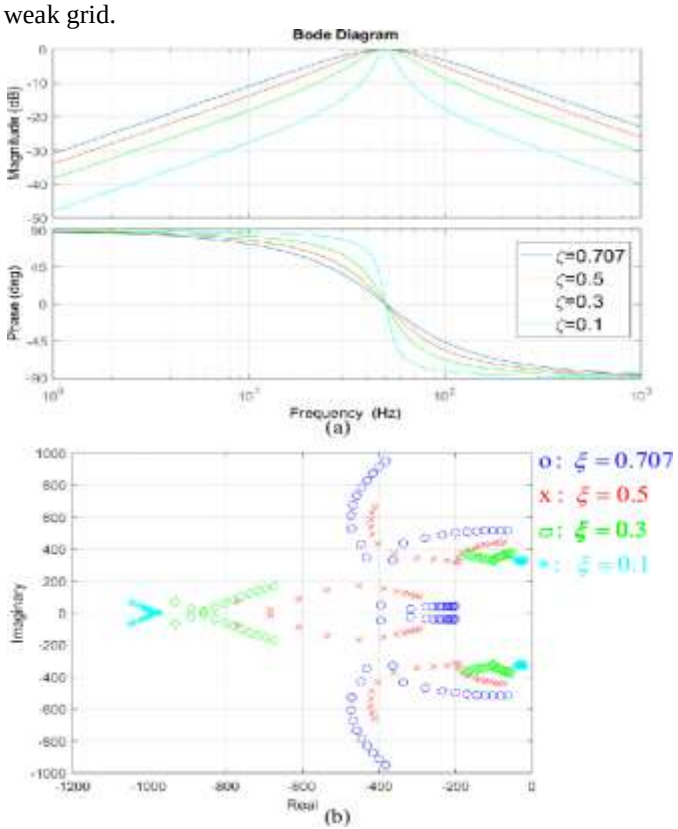

Fig. 9. Eigen values of the error dynamics when the damping ratio ζ is changed from 0.707 to 0.1, and $P^d = 3.5$kW and $Q^d = P^d$.

To check the robustness to the frequency variation, we change the grid frequency from 49 Hz to 51 Hz. In this case, we fix P^d = 3.5 kW and Q^d = 3.5 kvar, as shown in Fig. 8. We can observe that the eigenvalues move to the imaginary axis but all the eigenvalues of the closed-loop system are in the left-half plane. Moreover, to check the effect of the BPF to the proposed control method, we change ζ from 0.707 to 0.1. Fig. 9(a). shows the bode plot of the BPFs with different bandwidths. We can observe that part of the eigenvalues are closer to the imaginary when ζ is decreased, as shown in Fig. 9(b) However, all the eigenvalues remain in the left-half plane when P^d= 3:5 kW and Q^d = 3:5 kvar.

IV. RESULT ANALYSIS

To validate the proposed control method , we use the MATLAB/Simulink, Simscae power system. The parameters of the system used in the simulation are listed in Table I.

Table I
System Parameters Used In Simulations And Experiments

Parameter	Symbol	Value	Unit
Nominal grid voltage	$V_{ga,rms}$	110	V
Nominal grid frequency	f	50	Hz
Dc-link voltage	V_{dc}	730	V
Filter inductance	L	6	mH
Grid inductance	L_g	22	mH
Grid capacitance	C_g	15	μF
SCR	S_{cr}	1.5	pu
Resonance bandwidth of BPF	ω_c	222	rad/s
Resonance frequency of BPF	ω_0	314	rad/s
Switching frequency	f_{sw}	10	kHz

Fig. 10(a) shows PCC voltages ($V_{pcc, abc}$) performance of the VSI with the proposed control method when the power is constant. Fig. 10(b) shows Currents ($I_{L, abc}$) performance of the VSI with the proposed control method when the power is constant. Fig. 10(c). shows real and reactive power (P,Q) performance of the VSI with the proposed control method when the power is constant.

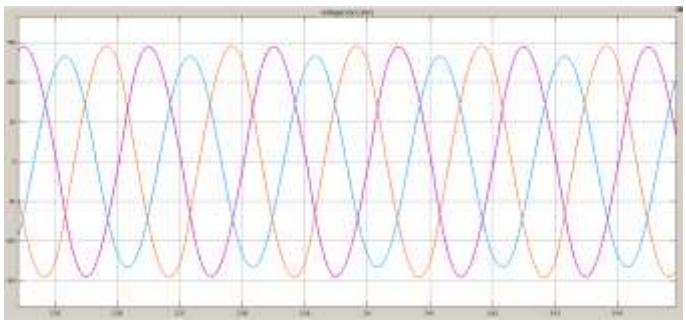

Fig. 10(a). PCC voltages ($V_{pcc, abc}$) when the power is constant.

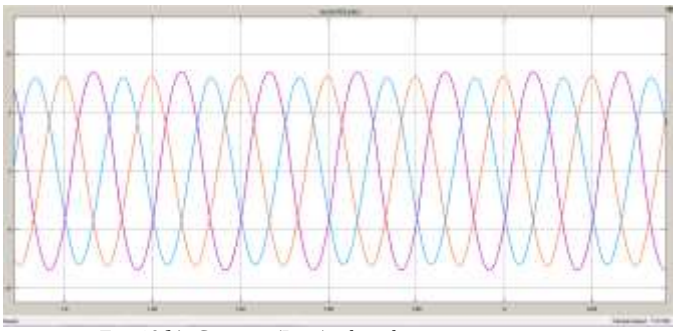

Fig. 10(b). Currents ($I_{L, abc}$) when the power is constant.

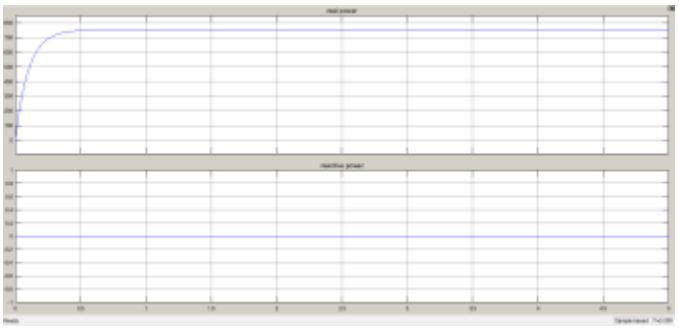

Fig. 10(c). Real and reactive power (P,Q) when the power is constant.

Fig. 11(a) shows PCC voltages ($V_{pcc, abc}$) performance of the VSI with the proposed control method when power vary at 2.5 second. Fig. 11(b) shows Currents ($I_{L, abc}$) performance of the when power vary at 2.5 second. Fig. 11(c). shows real and reactive power (P,Q) performance of the VSI with the proposed control method when power vary at 2.5 second.

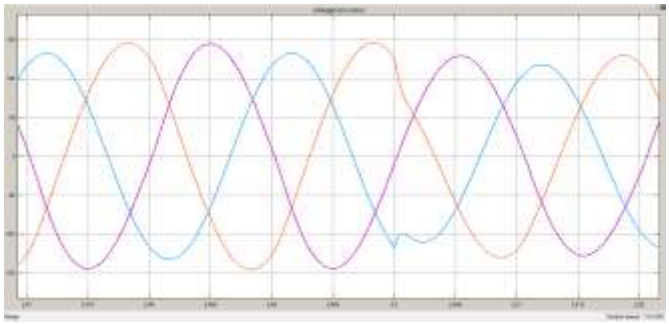

Fig. 11(a). Voltage ($v_{pcc, abc}$) when power vary at 2.5 second.

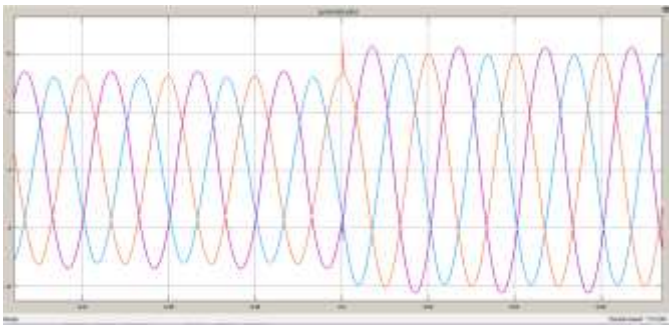

Fig. 11(b). Current ($I_{L, abc}$) when power vary at 2.5 second.

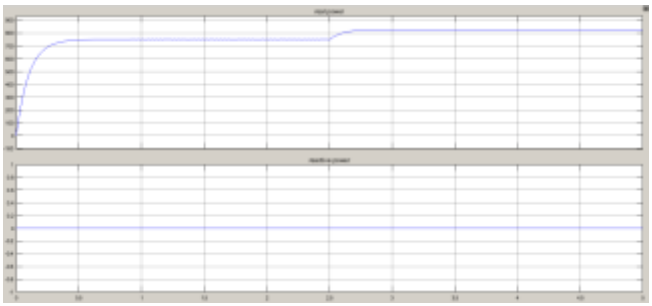

Fig. 11(c). Real and reactive power (P,Q) when power vary at 2.5 second.

Fig. 12. Shows Total Harmonic Distortion(THD) of the current 0.35% in case of start time 2.45 sec, number of cycles are 5, fundamental frequency 50 Hz, maximum frequency 1000Hz.

Fig. 13. shows the bode plot of the Band Pass Filters with different bandwidths. Bode diagram By varying the damping ratio ζ as 0.707, 0.5, 0.3 and 0.1.

V. Conclusion

In this study, we have eliminated the PLL which may make the system unstable. PLL is eliminated by a voltage modulated direct power control (VM-DPC) for a three phase voltage source inverter (VSI) connected to a weak grid. To apply the concept of GVM-DPC, we use a BPF for the weak grid- connected VSI system. However, from the eigen values based analysis we have seen that the system s always stable in this operating range. In addition, the system should generate some certain amount of reactive power to support the voltages at PCC as well, when we inject the rated real power to the weak grid. Finally, from the simulation results we have seen that the system is stable compared with the VCC method and the proposed method is working well in the weak grid.

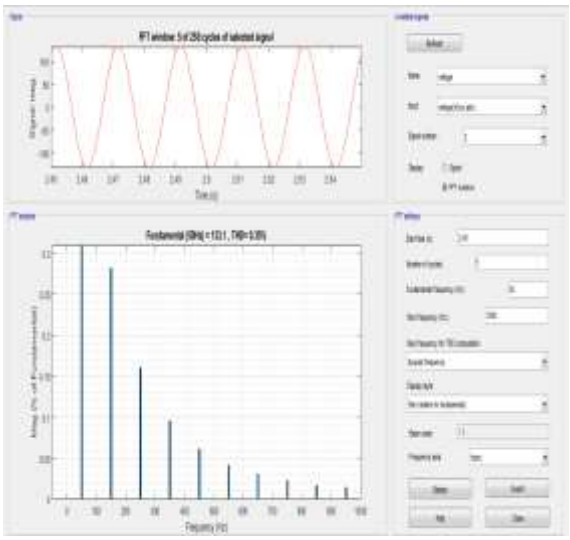

Fig. 12. Total Harmonic Distortion(THD)

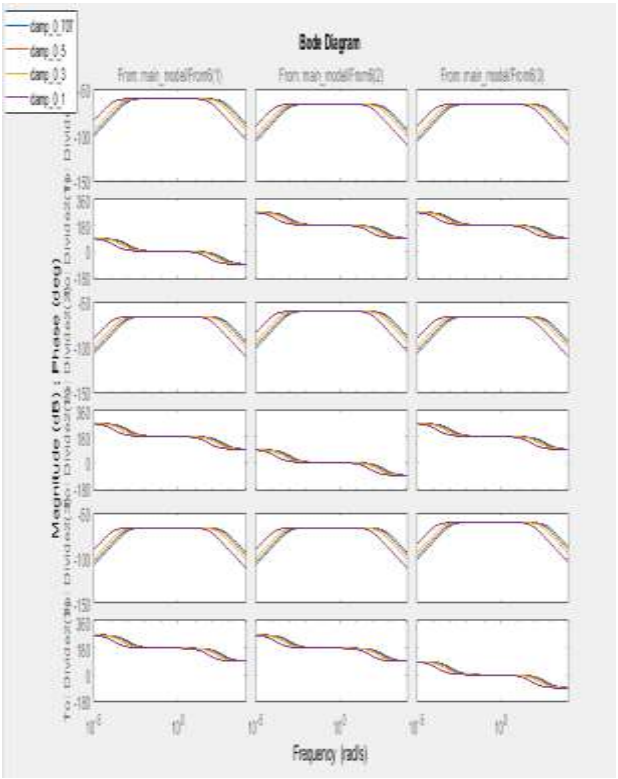

Fig. 13. Bode diagram By varying the damping ratio ζ as 0.707,0.5,0.3,0.1

References

[1] F. Blaabjerg, R. Teodorescu, M. Liserre, and A. V. Timbus, "Overview of control and grid synchronization for distributed power generation systems," IEEE Trans. Ind. Electron., vol. 53, no. 5, pp. 1398–1409, 2006.

[2] F. Blaabjerg, M. Liserre, and K. Ma, "Power electronics converters for wind turbine systems," IEEE Trans. Ind. Appl., vol. 48, no. 2, pp. 708– 719, 2012.

[3] Y. Gui, W. Kim, and C. C. Chung, "Passivity-based control with nonlinear damping for type 2 STATCOM systems," IEEE Trans. Power Syst., vol. 31, no. 4, pp. 2824–2833, 2016.

[4] F. Blaabjerg, Y. Yang, D. Yang, and X. Wang, "Distributed power generation systems and protection," Proc. IEEE, vol. 105, no. 7, pp. 1311–1331, 2017.

[5] F. Blaabjerg, Control of Power Electronic Converters and Systems, vol. 2. Academic Press, 2018.

[6] X. Guo, B. Wei, T. Zhu, Z. Lu, L. Tan, X. Sun, and C. Zhang, "Leakage current suppression of three-phase flying capacitor PV inverter with new carrier modulation and logic function," IEEE Trans. Power Electron., vol. 33, no. 3, pp. 2127–2135, 2018.

[7] Y. Gui, B. Wei, M. Li, J. M. Guerrero, and J. C. Vasquez, "Passivity based coordinated control for islanded AC microgrid," Appl. Energy, vol. 229, pp. 551–561, 2018.

[8] M. Kazmierkowski and L. Malesani, "Current control techniques for three-phase voltage-source PWM converters: a survey," IEEE Trans. Ind. Electron., vol. 45, no. 5, pp. 691–703, Oct. 1998.

[9] P. Rodr´ıguez, A. Luna, I. Candela, R. Mujal, R. Teodorescu, and F. Blaabjerg, "Multiresonant frequency-locked loop for grid synchronization of power converters under distorted grid conditions," IEEE Trans. Ind. Electron, vol. 58, no. 1, pp. 127–138, 2011.

[10] M. K. Ghartemani, S. A. Khajehoddin, P. K. Jain, and A. Bakhshai, "Problems of startup and phase jumps in PLL systems," IEEE Trans. Power Electron, vol. 27, no. 4, pp. 1830–1838, 2012.

[11] D. Dong, B. Wen, D. Boroyevich, P. Mattavelli, and Y. Xue, "Analysis of phase-locked loop low-frequency stability in three-phase grid-connected power converters considering impedance interactions," IEEE Trans. Ind. Electron., vol. 62, no. 1, pp. 310–321, 2015.

[12] M. Davari and Y. A.-R. I. Mohamed, "Robust vector control of a very weak-grid-connected voltage-source converter considering the phase locked loop dynamics," IEEE Trans. Power Electron., vol. 32, no. 2, pp. 977–994, 2017.

[13] B. Kroposki, B. Johnson, Y. Zhang, V. Gevorgian, P. Denholm, B.-M. Hodge, and B. Hannegan, "Achieving a 100% renewable grid: Operating electric power systems with extremely high levels of variable renewable energy," IEEE Power Energy Mag., vol. 15, no. 2, pp. 61–73, 2017.

[14] S.-K. Chung, "A phase tracking system for three phase utility interface inverters," IEEE Trans. Power Electron., vol. 15, no. 3, pp. 431–438, 2000.

[15] L. Harnefors, M. Bongiorno, and S. Lundberg, "Input-admittance calculation and shaping for controlled voltage-source converters," IEEE Trans. Ind. Electron., vol. 54, no. 6, pp. 3323–3334, 2007.

[16] L. Harnefors, X. Wang, A. G. Yepes, and F. Blaabjerg, "Passivity-based stability assessment of grid-connected VSCs–An overview," IEEE J. Emerg. Sel. Topics Power Electron., vol. 4, no. 1, pp. 116–125, 2016.

[17] B. Wen, D. Dong, D. Boroyevich, R. Burgos, P. Mattavelli, and Z. Shen, "Impedance-based analysis of grid-synchronization stability for threephase paralleled converters," IEEE Trans. Power Electron., vol. 31, no. 1, pp. 26–38, 2016.

[18] X. Wang, L. Harnefors, and F. Blaabjerg, "Unified impedance model of grid-connected voltage-source converters," IEEE Trans. Power Electron., vol. 33, no. 2, pp. 1775–1787, 2018.

[19] J. Z. Zhou, H. Ding, S. Fan, Y. Zhang, and A. M. Gole, "Impact of short-circuit ratio and phase-locked-loop parameters on the small-signal behavior of a VSC-HVDC converter," IEEE Trans. Power Del., vol. 29, no. 5, pp. 2287–2296, 2014.

[20] X. Wang and F. Blaabjerg, "Harmonic stability in power electronic based power systems: Concept, modeling, and analysis," IEEE Trans. Smart Grid, 2018, in press, DOI: 10.1109/TSG.2018.2812712.

[21] N. Bottrell, M. Prodanovic, and T. C. Green, "Dynamic stability of a microgrid with an active load," IEEE Trans. Power Electron., vol. 28, no. 11, pp. 5107–5119, 2013.

[22] X. Wang, F. Blaabjerg, and P. C. Loh, "Passivity-based stability analysis and damping injection for multiparalleled VSCs with LCL filters," IEEE Trans. Power Electron., vol. 32, no. 11, pp. 8922–8935, 2017.

[23] L. Harnefors, R. Finger, X. Wang, H. Bai, and F. Blaabjerg, "Vsc input-admittance modeling and analysis above the Nyquist frequency for passivity-based stability assessment," IEEE Trans. Ind. Electron., vol. 64, no. 8, pp. 6362–6370, 2017.

[24] T. Noguchi, H. Tomiki, S. Kondo, and I. Takahashi, "Direct power control of PWM converter without power-source voltage sensors," IEEE Trans. Ind. Appl., vol. 34, no. 3, pp. 473–479, 1998.

[25] M. Malinowski, M. Jasi´nski, and M. P. Kazmierkowski, "Simple direct power control of three-phase PWM rectifier using space-vector modulation (DPC-SVM)," IEEE Trans. Ind. Electron., vol. 51, no. 2, pp. 447–454, 2004.

[26] A. Bouafia, J.-P. Gaubert, and F. Krim, "Predictive direct power control of three-phase pulsewidth modulation (PWM) rectifier using space vector modulation (SVM)," IEEE Trans. Power Electron., vol. 25, no. 1, pp. 228–236, 2010.

[27] D. Zhi and L. Xu, "Direct power control of DFIG with constant switching frequency and improved transient performance," IEEE Trans. Energy Convers., vol. 22, no. 1, pp. 110–118, 2007.

[28] S. Vazquez, J. A. Sanchez, J. M. Carrasco, J. I. Leon, and E. Galvan, "A model-based direct power control for three-phase power converters," IEEE Trans. Ind. Electron., vol. 55, no. 4, pp. 1647–1657, 2008.

[29] J. Hu, L. Shang, Y. He, and Z. Zhu, "Direct active and reactive power regulation of grid-connected DC/AC converters using sliding mode control approach," IEEE Trans. Power Electron., vol. 26, no. 1, pp. 210–222, 2011.

[30] Y. Gui, G. H. Lee, C. Kim, and C. C. Chung, "Direct power control of grid connected voltage source inverters using port-controlled Hamiltonian system," Int. J. Control Autom. Syst., vol. 15, no. 5, pp. 2053–2062, 2017.

[31] S. Larrinaga, M. Vidal, E. Oyarbide, and J. Apraiz, "Predictive control strategy for DC/AC converters based on direct power control," IEEE Trans. Ind. Electron., vol. 54, no. 3, pp. 1261–1271, 2007.

[32] P. Antoniewicz and M. P. Kazmierkowski, "Virtual-flux-based predictive direct power control of AC/DC converters with online inductance estimation," IEEE Trans. Ind. Electron., vol. 55, no. 12, pp. 4381–4390, 2008.

[33] Z. Song, W. Chen, and C. Xia, "Predictive direct power control for three-phase grid-connected converters without sector information and voltage vector selection," IEEE Trans. Power Electron., vol. 29, no. 10, pp. 5518–5531, 2014.

[34] D.-K. Choi and K.-B. Lee, "Dynamic performance improvement of AC/DC converter using model predictive direct power control with finite control set," IEEE Trans. Ind. Electron., vol. 62, no. 2, pp. 757–767, 2015.

[35] S. Vazquez, A. Marquez, R. Aguilera, D. Quevedo, J. I. Leon, and L. G. Franquelo, "Predictive optimal switching sequence direct power control for grid-connected power converters," IEEE Trans. Ind. Electron., vol. 62, no. 4, pp. 2010–2020, 2015.

[36] Y. Gui, C. Kim, and C. C. Chung, "Grid voltage modulated direct power control for grid connected voltage source inverters," in Amer. Control Conf., pp. 2078–2084, 2017.

[37] Y. Gui, C. Kim, C. C. Chung, J. M. Guerrero, Y. Guan, and J. C. Vasquez, "Improved direct power control for grid-connected voltage source converters," IEEE Trans. Ind. Electron., vol. 65, no. 10, Oct. 2018.

[38] Y. Gui, M. Li, J. Lu, S. Golestan, J. M. Guerrero, and J. C. Vasquez, "A voltage modulated DPC approach for three-phase PWM rectifier," IEEE Trans. Ind. Electron., vol. 65, no. 10, pp. 7612–7619, Oct. 2018.

[39] Y. Gui, X. Wang, and F. Blaabjerg, "Vector current control derived from direct power control for grid-connected inverters," IEEE Trans. Power Electron., DOI 10.1109/TPEL.2018.2883507, pp. 1–1, 2018.

[40] H. Akagi, E. H. Watanabe, and M. Aredes, The instantaneous power theory. Wiley Online Library, 2007.

[41] F. Z. Peng and J.-S. Lai, "Generalized instantaneous reactive power theory for three-phase power systems," IEEE Trans. Instrum. Meas., vol. 45, no. 1, pp. 293–297, 1996.

[42] D. Yang, X. Wang, F. Liu, K. Xin, Y. Liu, and F. Blaabjerg, "Adaptive reactive power control of PV power plants for improved power transfer capability under ultra-weak grid conditions," IEEE Trans. Smart Grid, 2018, in press, DOI: 10.1109/TSG.2017.2762332.